Supplemental Information

Pneumatic Networks for Soft Robotics that Actuate Rapidly

Bobak Mosadegh[1,2], Panagiotis Polygerinos[3], Christoph Keplinger[1], Sophia Wennstedt[1], Robert F. Shepherd[1a], Unmukt Gupta[1], Jongmin Shim[3,b], Katia Bertoldi[3], Conor J. Walsh[2,3], and George M. Whitesides[1,2*]

[1] Department of Chemistry and Chemical Biology, Harvard University, 12 Oxford Street, Cambridge, MA 02138, USA.

[2] Wyss Institute for Biologically Inspired Engineering, Harvard University, 60 Oxford Street, Cambridge, MA 02138, USA.

[3] School of Engineering and Applied Sciences, Harvard University, Cambridge, MA 02138, USA.

(*) Correspondence should be addressed to: gwhitesides@gmwgroup.harvard.edu

Fabrication of fPN Actuator

The fPN actuators were made similarly to sPN actuators, as described previously [1-3].

First, molds were made in acrylonitrile butadiene styrene (ABS) using a three-dimensional (3D)

printer (Dimension 3D; Stratasys, Inc.) based on a computer-aided-design (CAD) drawing

(Solidworks Corp, Waltham, MA). The fPN actuator required three molds: an interior and

exterior mold for the top extensible layer and a third mold for the bottom inextensible layer

(Fig. S1). The interior mold consisted of chambers connected by a single channel, so that all

chambers inflate simultaneously. The connecting channel had a smaller height (1 mm) than the

chambers (10.5 mm); this difference caused the chambers to expand preferentially when

pressurized. The features of the exterior mold consisted of straight parallel plates that fit in

between each chamber of the interior mold. The plates separate the elastomeric material

between each chamber such that no two chambers shared an inside wall.

We fabricated the bottom layer by pouring elastomer in a flat mold that contained a

piece of paper, which served as the inextensible material. The top layer was placed inside the

bottom layer before curing so that the elastomer was cured in place. Alternatively, the paper

can be bonded after curing of the bottom layer using a silicone adhesive such as Elastosil E951

(Wacker Chemical Corp., Adrian, Michigan) (Fig. S1C). We used two types of elastomers, Ecoflex

30 (Smooth-On Inc., Easton, PA) and Elastosil M4601 (Wacker Chemical Corp., Adrian,

Michigan), which are both two-component silicone rubbers that polymerize at room

temperature. Ecoflex 30 is extremely soft (shore value of 00-30) and Elastosil M4601 is

relatively stiff (shore A30). We made inlet holes using a 2-mm biopsy punch at one end of the

actuator. Using tubing of a slightly larger diameter (1/32" inner, 3/32" outer) than the inlet

provided an adequate seal. Actuators were pressurized by compressed air or nitrogen supplied by gas tanks. Hydraulic actuation was also performed using water supplied by a syringe pump.

Characterization of fPN actuator

We tested the various designs of the fPN actuators by measuring the pressure required to bend them fully (Fig. S2). We used a pressure regulator (Type 700, Control Air Inc., Amherst, NH) to control the delivery of pressurized gas to the actuator. We considered an actuator fully bent when both ends of the actuator were in contact. A pressure gauge (MGA-30-A-9V-R, SSI technology Inc., Janesville, WI), directly connected to the actuator by tygon tubing (1/32" inner, 3/32" outer), displayed the pressure. We captured images of the actuators in their bent positions using a Nikon D5100 camera.

Pressure-Volume (PV) curves

We generated PV hysteresis curves by hydraulic inflation and deflation of the actuators in a 10-gallon fish tank. We fixed a syringe pump (Harvard Apparatus, PHD 2000) and pressure sensor (Transducers Direct, TDH30) in an orientation parallel to the surface of the water (Fig. S3). We clamped the actuator fully submerged in the water in a vertical position and placed a grid (2.5 x 2.5 mm) behind it for reference. We filled the actuators with water by submerging them in water and applying a vacuum several times until bubbles would no longer emerge (squeezing the actuators under water also enabled effective removal of air).

Within each test, we switched from inflation to deflation when the actuator had achieved full bending, which we considered to be when the free end of the actuator touched its fixed end, and thus created a full circle. Once the actuator had completed one full cycle and

the pressure returned to zero, we inflated it again to assure reproducibility. We repeated this procedure for at least three cycles.

Finite Element Model of the sPN/fPN actuator

To investigate the distribution of strains during actuation in the sPN and fPN actuators we built 3D models and used the commercial finite element (FE) software Abaqus FEA for the analysis, employing the the Abaqus/Standard solver. The geometry of the actuator was imported into Abaqus CAE as a stl file and meshed using solid quadratic tetrahedral elements (Abaqus element type C3D10H) for all the elastomeric components of the actuators and shell elements (Abaqus element type STRI65) for the inextensible layer of paper. The accuracy of each mesh was ascertained through a mesh refinement study, resulting in a model with 19,826 solid and 738 shell elements for the case of the sPN actuator and 26,593 solid and 845 shell elements for the case of the fPN actuator.

To capture the response of the elastomer used to fabricate the actuators (Elastosil), we modeled the material as a hyper-elastic solid and computed the stresses and elastic energies using the nearly-incompressible Yeoh model,[4] whose strain energy density is given by

$$U = \sum_{i=1}^{N} C_{i0} \left(\bar{I}_1 - 3 \right)^i + \sum_{i=1}^{N} \frac{1}{D_i} \left(J - 1 \right)^{2i} \tag{1}$$
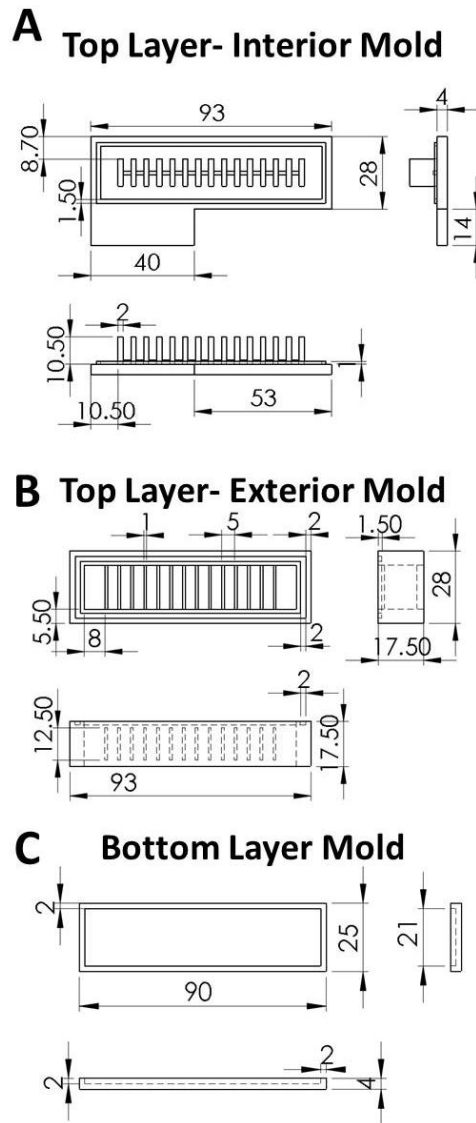
where $\bar{I}_1 = tr[dev(\mathbf{FF})^T]$, $J = \det(\mathbf{F})$, and $\mathbf{F}$ is the deformation gradient and C_{i0} and D_i are the materials parameters. Here, we used N=3 and C_{10}=0.11, C_{20}=0.02, C_{30}=0, D_1=D_2=D_3=0.

Moreover, the response of the inextensible layers was captured using a linear elastic model with a Young's Modulus of 6.5 GPa and a Poisson's ratio of 0.2.
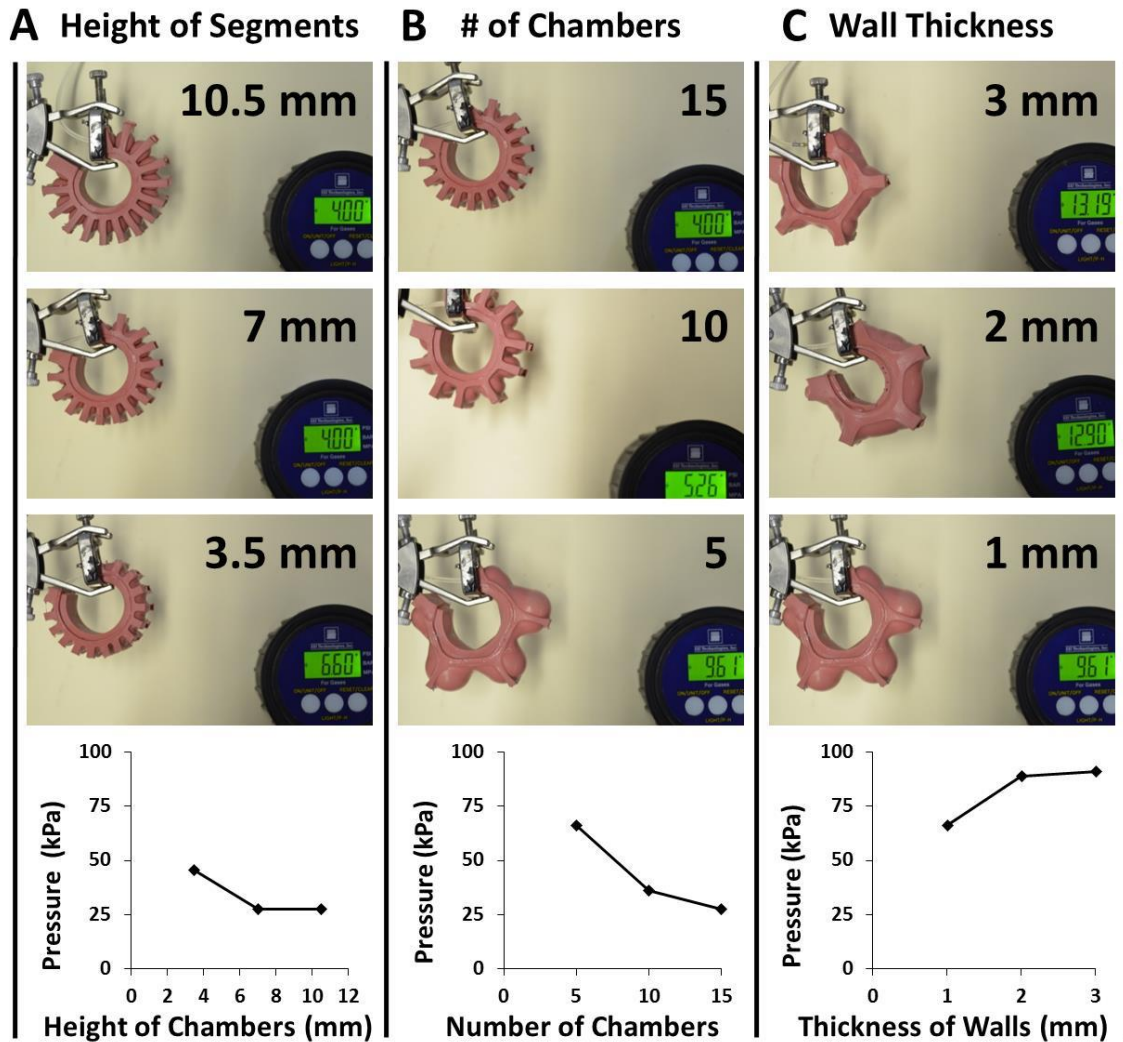
Thereafter, static simulations were performed applying pressure on all internal faces of the cavities and assuming zero displacements at the top and bottom face of the proximal pneu-net chamber to simulate the experimental boundary conditions. Gravitational forces were taken into account in the simulations.

Characterizing the Rapid Actuation of fPNs

To demonstrate the rapid actuation of the fPN, we incorporated multiple sensing modalities (pressure/flow sensors and high definition cameras) to obtain information on the performance of the fPNs. Using this system, we mounted one end of the fPN on a rigid fixture so it could perform its full range of bending without any obstruction by the fixture. A source of regulated (P31-pressure regulator, Parker Hannifin Corp.) pressurized air was connected to the actuator. Two solenoid valves (X-Valve, Parker Hannifin Corp.) supplied and vented the air. A graphical user interface (LabView 2012, National Instruments) controlled the pressure regulator and monitored the flow rate (AWM5000, Honeywell) and pressure (ASDX Series, Honeywell) of air transferred to and from the actuator. A data acquisition card (NI USB-6211, National Instruments) interfaced the hardware and software and regulated the timing of the valves through electronic relays (SRD-05VDC-SL-C Power Relay, Songle Relay Co.).

Supplemental Figure S1. Molds for Fabricating a fPN Actuator. A) Dimensions (mm) for the interior mold for the top layer of the fPN actuator. Shown are 2D sketches of the top, side, and back views of the molds. B) Dimensions for the exterior mold for the top layer of the fPN actuator. Shown are 2D sketches of the bottom, side, and back views. C) Dimensions for the mold for the bottom layer of the fPN actuator. Shown are 2D sketches of the top, side, and back views.

Supplemental Figure S2. fPNs of Different Geometries. A-C) Pressure each actuator required to bend fully (gauges show pressure in psi). A) Varied channel height with a constant number of chambers (15) and thickness of chamber inside walls (1 mm). B) Varied number of chambers with a constant height of chambers (7 mm) and wall thickness (1 mm). C) Varied thickness of inside walls with constant height of chambers (10.5 mm) and number of chambers (5).
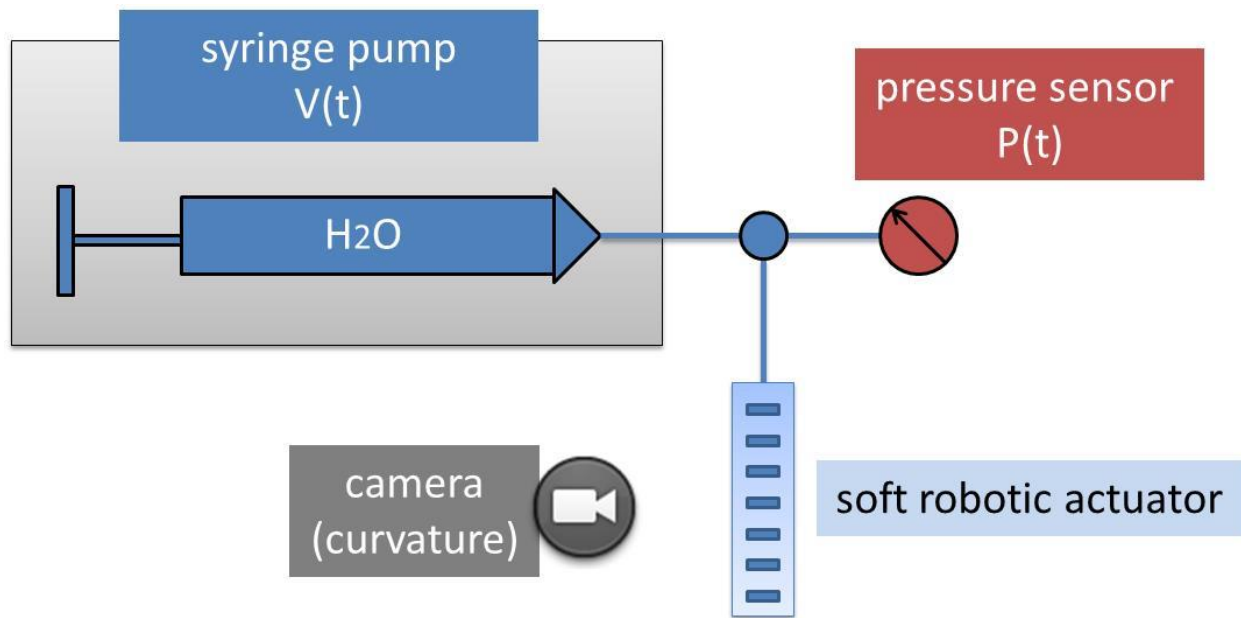
Figure S3. Experimental System to Measure Pressure-Volume Hysteresis Curves. A programmable syringe pump infuses water to a T junction that was connected to a pressure sensor and the soft robotic actuator. Due to the incompressibility of water, the rate of infusion of the syringe pump was directly related to the changes in volume of the pneumatic channels of the actuator. Rates of infusion were chosen to be sufficiently low to achieve quasistatic conditions. To minimize the effect of gravity, the actuator was suspended in water within a fish tank made of glass. Bending of the actuator was monitored by a webcam.
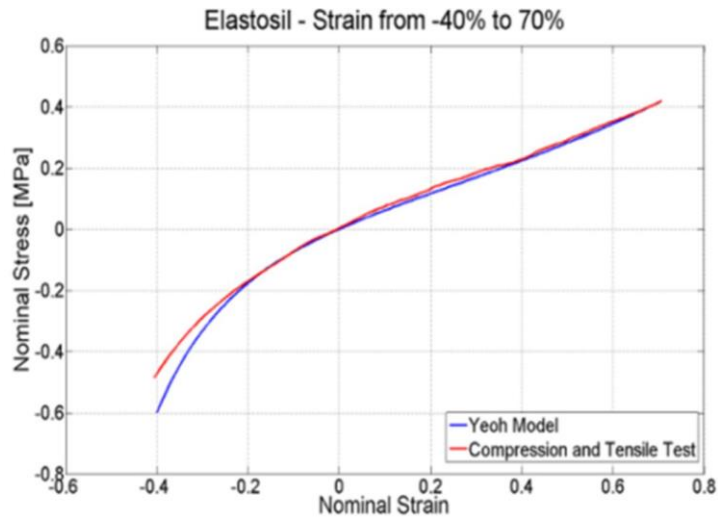
Figure S4. **Stress-Strain Curve of Elastosil M4601**. Compression and tensile tests of the elastomeric material (Elastosil M4601) used for simulations of the actuators. The stress-strain curve is fitted with the Yeoh model of hyperelasticity.
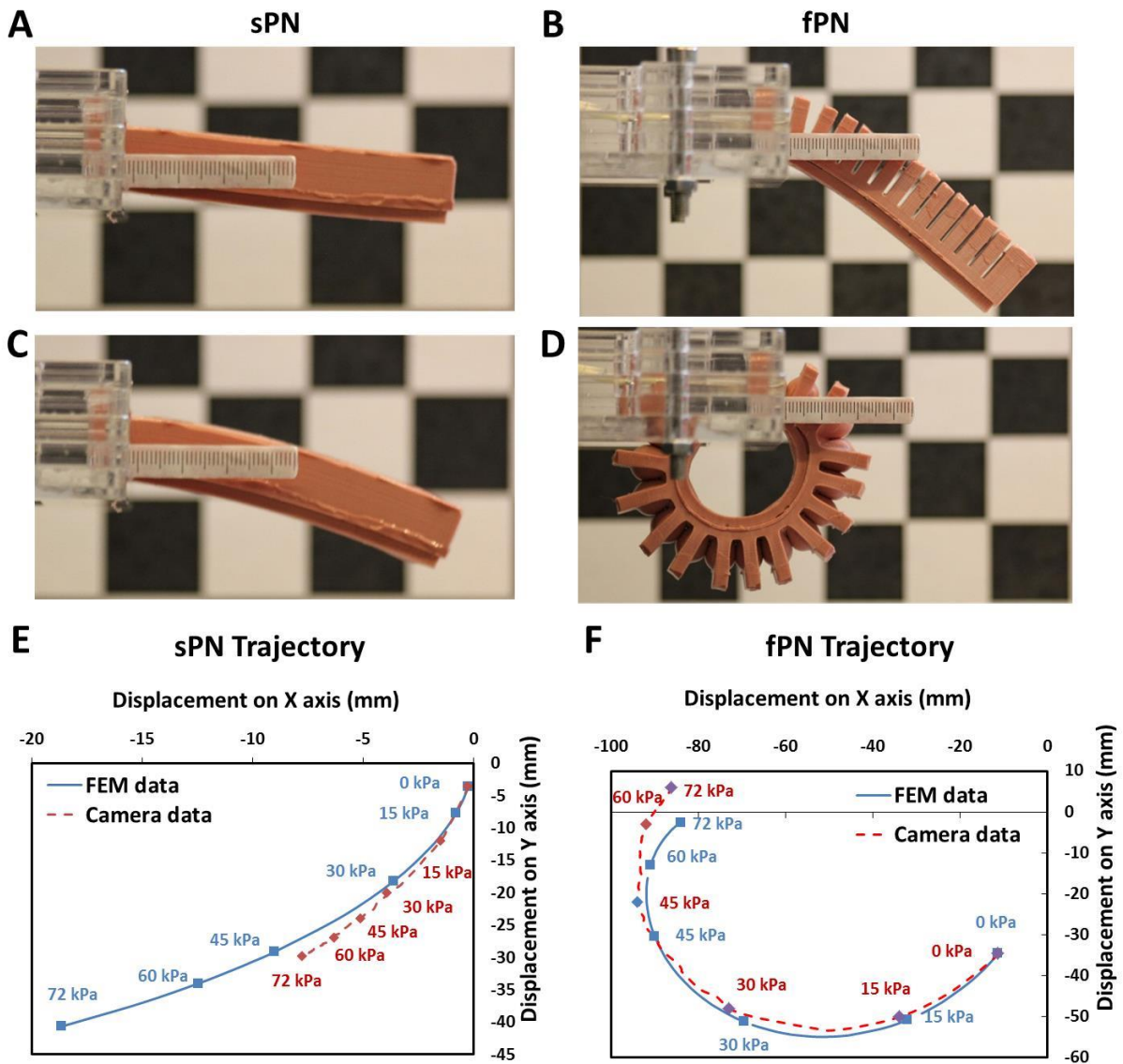
Figure S5. Bending of sPN and fPN actuator. A-D) Images of sPN (A,C) and fPN (B,D) actuators when pressurized with 0 kPa (0 psi) (A,B) and 72 kPa (10.44 psi) (B,D). Marks on the scale bar represent mm. E-F) Plot of trajectories for experimental and FEM tests for the tip of the free end of the sPN and fPN actuators at various pressures.
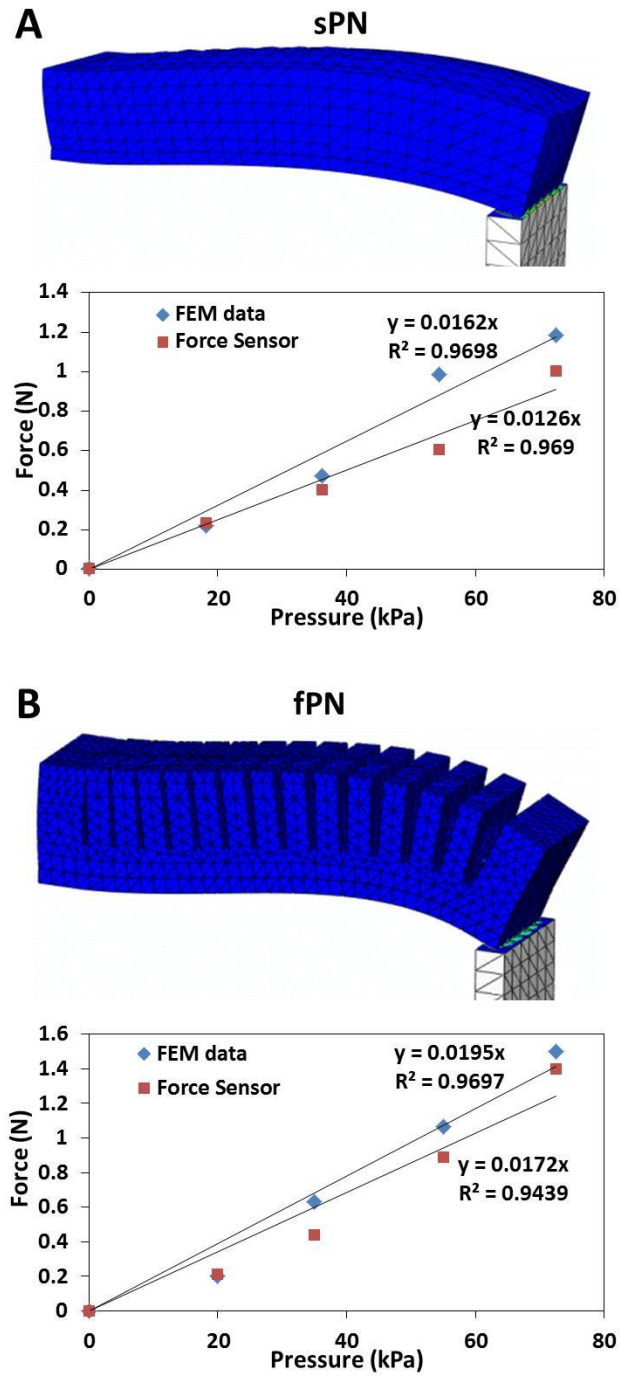
Figure S6. Force Exerted at Tip of Pneu-net. A-B) FEM model of a sPN (A), and fPN (B) to simulate the force exerted at its tip for several pressures. Plot includes data from both simulated and experimental measurements.

References

1. F. Ilievski, A. D. Mazzeo, R. F. Shepherd, X. Chen and G. M. Whitesides, *Angew. Chem. Int. Ed.*, **2011**, 50, 1890.

2. R. F. Shepherd, F. Ilievski, W. Choi, S. A. Morin, A. A. Stokes, A. D. Mazzeo, X. Chen, M. Wang and G. M. Whitesides, *Proc. Natl. Acad. Sci. U.S.A.*, **2011**, 108, 20400.

3. R. F. Shepherd, A. A. Stokes, J. Freake, J. Barber, P. W. Snyder, A. D. Mazzeo, L. Cademartiri, S. A. Morin and G. M. Whitesides, *Angew. Chem. Int. Ed.*, **2013**, 52, 2892.

4. O. H. Yeoh, *Rubb. Chem. Tech.*, **1993**, 66, 754.